Acidic Processing of Fly Ash: Chemical Characterization, Morphology, and Immersion Freezing

1
2
3
4
5
6
7
8
9
10
11
12
13
14
15
16
17
18
19
20
21
22
23
24
25
26
27
28
29
30
31
32
33
34
35
36
37
38
39
40
41
42
43
44
45
46
47
48
49
50
51
52
53
54
55
56
57
58
59
60

Acidic Processing of Fly Ash: Chemical Characterization, Morphology, and Immersion Freezing

Delanie J. Losey[1,%], Sarah K. Sihvonen[1,#], Daniel P. Veghte[1,&], Esther Chong[1], and Miriam Arak Freedman[1]*

(1) Department of Chemistry, The Pennsylvania State University, University Park, PA 16802

* To whom all correspondence should be addressed: maf43@psu.edu, 814-867-4267

% Present address: DuPont, Circleville, OH 43113

Present address: Syngenta, Greensboro, NC 27419

& Present address: William R. Wiley, Environmental Molecular Sciences Laboratory, Pacific Northwest National Laboratory, Richland, WA 99354

ABSTRACT

Fly ash can undergo aging in the atmosphere through interactions with sulfuric acid and water. These reactions could result in chemical and physical changes that could affect the cloud condensation or ice nucleation activity of fly ash particles. To explore this process, different water and acid treated fly ash types were characterized with x-ray diffraction (XRD), transmission electron microscopy (TEM), electron dispersive spectroscopy (EDS), selected area diffraction (SAED), and inductively coupled plasma atomic emission spectroscopy (ICP-AES). Then, their immersion freezing activity was assessed. With water and acid treatment, a wide variety of metals were leached, depending on the starting composition of the fly ash. Acid treatment resulted in the formation of gypsum, $Ca(SO_4) \cdot 2H_2O$, for fly ash containing Ca as well as morphological changes. The immersion freezing activity was also assessed for each fly ash system to compare the effects of water and acid processing. Our results support the assertion that fly ash can serve as a cloud condensation or ice nucleus to affect climate.

ENVIRONMENTAL SIGNIFICANCE

Heterogeneous nucleation is an important process in the atmosphere for the formation of ice-containing clouds because it allows ice to form at temperatures warmer than -38 ºC. Fly ash and sulfuric acid are emitted into the atmosphere as byproducts of coal combustion. Fly ash may be an important species for heterogeneous ice nucleation, and its interaction with sulfuric acid may alter its ice nucleation efficiency. Its ice nucleation activity, however, may be complex because fly ash has a heterogeneous composition where some types of fly ash are enriched in calcium and/or iron, which could also impact its ability to nucleate ice. The data presented give insight

1
2
3
4
5
6
7
8
9
10
11
12
13
14
15
16
17
18
19
20
21
22
23
24
25
26
27
28
29
30
31
32
33
34
35
36
37
38
39
40
41
42
43
44
45
46
47
48
49
50
51
52
53
54
55
56
57
58
59
60

into the changes that occur to composition and morphology when fly ash is exposed to water and acid, and the impact of this processing on its activity towards ice nucleation.

INTRODUCTION

Aerosol particles can serve as seeds for cloud condensation and ice formation. The magnitude of the impact of aerosol – cloud interactions on climate is highly uncertain.[1] One common cloud type are mixed-phase clouds, which are composed of super-cooled water and ice particles.[2] These clouds are of particular interest due to their ability to impact climate and the hydrological cycle.[3-5] They can be found roughly in the region where the temperature is lower than -5 ºC but higher than -38 ºC, below which homogeneous freezing becomes predominant.[6, 7] Because of this temperature range, heterogeneous ice nucleation is the primary pathway for ice formation within these clouds. As a result, properties of the substances that can serve as ice nuclei, such as mineral dust, salts, biological species, and ash particles have been and continue to be extensively studied. [2, 8-12]

Combustion processes contribute significantly to aerosol emission across the globe.[13-15] In particular, black carbon is thought to be the second largest anthropogenic climate forcing agent after CO_2.[10] The combustion of coal produces many other materials that are emitted into the atmosphere, one of which is fly ash, a major byproduct of the coal burning process. Although efforts are made to control the fly ash with filtration and adsorbent systems, large quantities of fly ash are emitted into the atmosphere.[16] Fly ash is commonly found as a combination of crystalline and amorphous components that primarily contains oxides of silica, aluminum, calcium, and iron, which can also be found in mineral dust, a common type of aerosol particle.[16, 17] Fly ash particles are alkaline because they contain CaO and MgO.[14]   The composition and

morphology of fly ash differ based on the type of coal.[16] Fly ash can be described as Class C, resulting from the burning of lignite or sub-bituminous coal, or Class F, resulting from the burning of anthracite or bituminous coal. The classes are also distinguished by their composition, in which Class C has CaO content that may approach 30-40% and 20% for Class F. Additionally, Class F must have a sum of SiO_2, Al_2O_3, and Fe_2O_3 equal or greater than 70%.[18, 19] Due to their different compositions, it is important to explore each fly ash type as their reactivity and ice nucleation activity are expected to differ.[20] Because most fly ash particles are submicron in size, they can undergo long range atmospheric transport.[21] In addition to the size, the composition of the fly ash can have an impact on the transport.[22, 23] For example, fly ash that contains high concentrations of water-soluble components may become CCN and sediment out. During transport, fly ash can be involved in heterogeneous chemistry, such as acidic processing, which can alter its properties and ability to form cloud droplets and/or nucleate ice. Exposure to acidic materials is likely since SO_2 and NO_2, precursors of sulfuric and nitric acid, are co-emitted with fly ash. Acidic processing of fly ash results in leaching of metals such as Al, Fe, and Mg.[24-26] Navea et al. suggested that the OH density in particular, which varies based on the fly ash location, affects the water adsorption and ice nucleation activity of the fly ash.[20] In conjunction with composition, surface properties can have an impact on the ice nucleation activity. Hiranuma et al. has shown that milled hematite, which has more surface features caused by the milling process, has enhanced ice nucleation activity compared to synthesized hematite.[27]

Previous studies that focused on the ice nucleation activity of fly ash have found that fly ash can serve as an efficient ice nucleus in immersion and condensation freezing.[21, 28, 29] Due to the water-soluble components that could be found on the surface of fly ash, immersion (when the particle is in a water droplet) and/or condensation freezing (when water condenses and freezes) is

likely. In comparison to mineral dust aerosol, which has more crystalline structures, fly ash possesses some glassy (or amorphous) components, which may affect the ice nucleation activity. Of the few studies that have explored ice nucleation of fly ash, three of them focused on immersion freezing behavior and found that fly ash can serve as immersion nuclei.[28, 29] Umo et al. investigated different types of combustion ashes and hypothesized that the ice nucleation activity was related to the composition (e.g. the quartz content).[28] Likewise, Grawe et al. (2016) proposed a composition dependence when investigating immersion freezing of ash from wood and lignite coal burning.[29] In later research on fly ash, Grawe et al. (2018) studied the effect of dry versus wet generation of their samples before performing ice nucleation experiments. They observed that the generation method could have an effect on the ice nucleation efficiency of the sample.[30] Another study by Zawadowicz et al. used nitric acid to treat the same fly ash samples as this study, but their objective was to improve their single particle mass spectrometry detection methodology for biological aerosol particles and did not further analyze the effects of the nitric acid on their samples. Based on their spectra, the nitric acid did not show any noticeable changes in the composition from the untreated samples.[31] Although done at very acidic conditions, Blanco et al. saw that the acid leaching of two fly ash samples led to the depletion of CaO, Fe_2O_3, Al_2O_3 but little change in the quartz weight percent after one hour in 30 wt. % sulfuric acid.[32]

In this study, the physical and chemical properties of four fly ash samples representative of emissions from around the United States are explored before and after acid treatment. The effect of exposing different types of fly ash to sulfuric acid on the ice nucleation ability of fly ash has not previously been explored despite the co-location of the two substances. Sulfuric acid coatings and treatment have been extensively investigated on mineral dust, where it is found that sulfuric

acid decreases the ice nucleation efficiency in both immersion and deposition freezing modes.[33-39] To determine changes to composition, inductively coupled plasma-atomic emission spectroscopy (ICP-AES) was used. To identify the components and determine changes to crystallinity, X-ray diffraction (XRD), transmission electron microscopy (TEM) with selected area electron diffraction (SAED) and energy dispersive spectroscopy (EDS), and Brunauer-Emmett-Teller (BET) surface area measurements were taken. Immersion freezing was used to explore the effect of acid processing on the freezing properties of fly ash. The effects of sulfuric acid treatment and water treatment are investigated and are discussed in the context of atmospheric processing.

EXPERIMENTAL METHODS

Four fly ash samples of three different Class types were chosen. Two Class C fly ash samples, Joppa (Joppa Generating Station, Joppa IL) and Welsh (Welsh Generation Station, Pittsburg, TX), a hybrid Class C/F fly ash, Clifty (Clifty Creek Power Plant, Madison, IN), and a Class F fly ash, Miami (Miami Fort Generation Station, North Ben, OH) were used for these studies. All fly ash samples were obtained through Fly Ash Direct, a service of Waste Management, Inc. The initial, untreated samples were sent to Resource Materials Testing Inc., where the elemental compositions for each fly ash sample were determined using wet chemical techniques as specified by regulatory guidelines (Table 1).[19] The fly ash was treated with sulfuric acid or water following the same procedure and called acid treated and water treated, respectively. Fly ash (0.4 g) was combined with sulfuric acid (0.10 M, 15 mL; EMD, ACS Reagent grade) or ultrapure water (15 mL, HPLC grade, Fisher). After being stirred for 1.5 hours, the samples were centrifuged and the supernatant was decanted for analysis with ICP-AES. Note that some of the liquid remains in the sample after centrifugation. The fly ash was allowed to dry by evaporation

for several days. The solid was lightly ground with a mortar and pestle before analysis by TEM, XRD, and Brunauer-Emmett-Teller (BET) analysis.

The pH of 0.10 M sulfuric acid was selected to be representative of aqueous processing in the atmosphere. It has been seen in several studies that atmospheric fine particles can have pH ranges from -0.51 to 3.1 and up to 4.9 for haze and biomass burning events.[40-43] A concentration of 0.1 M H_2SO_4 was chosen because it corresponds to a pH of 0.7, which falls into this range. Compared to our fly ash samples, in the atmosphere, the ions leached out of the particles would not generally be washed away, but instead, would be found in the aqueous solution. Nonetheless, our samples are good mimics of aqueous processing in the atmosphere but not an exact representation.

The samples were each submitted for BET analysis to determine surface area with N_2 as the flow gas. Pore size was determined from BET using the Gurevitsch method, which assumes all pores are uniform cylinders.[44] Additionally, pH measurements of the 0.3 wt. % suspended solutions of the lightly ground samples were taken with a pH meter (B30PCI/89231-580, VWR International) and can be found in Table S1. Because sample preparation includes centrifuging and sonication before immersion freezing experiments, the fly ash samples may undergo chemical and morphological changes that would not be accounted for with untreated samples. Thus, for our experiment, the water treated fly ash is a better comparison to the acid treated than the untreated fly ash for the immersion freezing data. For the ice nucleation on gypsum (>98%, MP Biomedicals) and quartz (Research grade, Ward's Natural Science Establishment, Inc.), the procedure followed that of the fly ash samples after their treatments. The minerals are ground in a mortar and pestle to a fine powder and then dispersed in Millipore water (0.3 wt. %) by magnetic stirring.

For the XRD experiments, an X-ray diffractometer with Cu Kα radiation with a current of 40 mA and a voltage of 45 kV was used. Bulk powder samples were front loaded in a zero-background silicon holder. Goniometer angles were set from 5 to 70° 2θ with a 0.0263° 2θ step size and a scan step time of 96.4 s. A beam knife was used to reduce low angle scattering. The diffractograms (Figure 1) range from 5-45° instead of ranging to 70° because of the higher intensity found at the lower angles and well-defined peaks. Although there were some defining peaks at the higher angles, the intensity decreases, which makes it difficult to distinguish the peaks for these highly complex samples. The XRD diffractograms were analyzed using Jade XRD libraries.

Samples for TEM were prepared using particles that were dry-generated from the untreated and acid-treated minerals, which were impacted on continuous carbon coated copper mesh grids (CF200-CU, Electron Microscopy Sciences, Hatfield, PA, USA) using a cascade impactor (PIXE International Corp. Tallahassee, FL, USA). The dry-generation method consisted of a vial containing the dried, lightly ground fly ash samples that are entrained with a flow of dry N_2 gas into the cascade impactor that is backed with a pump at 1.0 lpm.[39, 45-47] An average of 30 particles were imaged ranging from 50 nm to 3 μm, and representative morphologies were analyzed with SAED and EDS. During the TEM analysis, SAED and EDS were performed to investigate the degree of crystallinity and the elemental composition of individual particles, respectively.

The immersion ice nucleation experiments were performed using the lab-built immersion freezing chamber, which has been described in detail in Alstadt et al.[48] Droplets containing the dried, lightly ground fly ash (0.3 wt.%, 2μL) in ultrapure water (Millipore Q, 18 MΩ) were pipetted onto a hydrophobically coated slide (Hampton research), which was then placed inside

the chamber. Four trials were run for each sample with a minimum total of 120 droplets studied for each sample. The chamber was cooled by flowing nitrogen gas through a copper coil submerged in liquid nitrogen, while images were captured every 0.5 °C. The flow was adjusted to allow for a 3 °C /min cooling rate. We assume the droplets are sufficiently large to minimize evaporation over the timescale of the experiment. Broadley et al. previously found no dependence on the cooling rate between 0.8 and 10 °C/min with NX-illite particles.[49]

The number of droplets frozen at a given temperature (n(T)) were recorded to calculate the cumulative fraction of droplets frozen (f_{ice}) using the following equation:

$$f_{ice} = \frac{n(T)}{N} \qquad (1)$$

where N is the total number of droplets. In order to rule out background freezing from the Millipore water, freezing experiments were performed with pure Millipore water (206 particles in total). Using the procedure outlined in O'Sullivan et al. and based on Vali et al., the fraction of droplets frozen at a specific temperature, F(T), from each trial was used to calculate K(T), the number of nucleation sites per milliliter water at that temperature for each Millipore and fly ash trial as follows:

$$K(T) = \frac{-\ln[1-F(T)]}{V} \times d \qquad (2)$$

where V is the droplet volume in milliliters and d is the dilution factor.[50, 51] The average K(T) at each temperature for the Millipore water is then subtracted from the average K(T) calculated for each fly ash experiment. The number of surface sites per unit area as a function of temperature (n_s) is calculated from the K(T) using the following equation:

$$n_s = K(T) \times C^{-1} \qquad (3)$$

where C is the total surface area of fly ash in a given volume, which is calculated using the BET surface area and mass percent fly ash in each experiment. The n_s is calculated at each

temperature and its standard deviation is calculated using the standard deviation of K(T) over each trial.

RESULTS AND DISCUSSION

The fly ash used in this study is classified into 3 categories: Class C, Class F, and a hybrid Class C/F. The samples were sent to Resource Materials Testing Inc., and the elemental compositions for each fly ash sample were determined using wet chemical techniques as specified by regulatory guidelines.[19] As seen in Table 1, Si is the primary component of all fly ash (46.47 – 34.03%) with Al also being a major component (18.23 – 21.50%). Class C fly ash, Joppa and Welsh, have a high amount of Ca (24.27% and 26.89%, respectively). Class F has the smallest amount of Ca (3.41%), but the highest amount of Fe (22.17%). Class C/F has almost equal amounts of Ca and Fe (11.78% and 12.39%, respectively). To a lesser extent, Mg, Na, K, and S are also present in every fly ash type. Note that the metal elements are listed as their most common oxides in Table 1 due to the analysis method used by Resource Materials Testing Inc. and may not have the same composition in the sample as indicated by the chemical formula listed.[19]

Table 1. The percent composition by mass of the fly ash samples from Resource Materials Testing Inc.,[19] and the crystalline fly ash components identified using XRD (marked with an *).

Chemical	Name	Class C		Class C/F	Class F
		Joppa (%)	Welsh (%)	Clifty (%)	Miami (%)
SiO_2	Quartz	38.84*	34.03*	43.13*	46.47*
Al_2O_3	Alumina	19.53	18.23	21.31	21.50
Fe_2O_3	Hematite	5.44	5.68*	12.39*	22.17*

CaO	Lime	24.27*	26.89*	11.78*	3.41*
MgO	Periclase	4.88*	6.32*	2.51*	1.02*
Na_2O		1.62	2.52	2.22	0.64
K_2O		0.69	0.42	1.34	2.32
SO_3		1.42	1.98	2.82	1.13
$Al_{2.35}Si_{0.64}O_{4.82}$	Mullite	---*	---*	---*	---
Fe_3O_4	Magnetite	---*	---	---*	---*
$CaSO_4$	Anhydrite	---*	---*	---*	---
$CaCO_3$	Calcite	---*	---*	---*	---
Products after acid treatment					
$Ca(SO_4)\cdot 2H_2O$	Gypsum	---*	---*	---*	---

The XRD results determine the crystalline phases present in each fly ash sample before and after reaction with sulfuric acid. Table 1 and Figure 1 show the results of this analysis. The diffractograms' ranges were limited to 45°. At angles greater than 45°, the intensity decreases and the peaks are less defined making it difficult to differentiate the peaks when labelling. Thus, only the major components in the XRD diffractograms were labelled for clarity. A representative full diffractogram can be seen in Figure S1. The results indicate that both crystalline and amorphous components are present. The Class C/F Clifty and Class F Miami samples have the most amorphous material, indicated by the large humps in the background of each sample that can be seen around 10° and 25°. The amount of amorphous content in the samples could be quantified if an external crystalline standard had been used. Rietveld refinement was attempted on the samples for composition data, but the goodness of fit values were too large to be considered as accurate fits. Therefore, the components of each fly ash sample were not quantified, but major and minor components can be determined. For all samples, the primary

crystalline component of each sample is quartz (SiO_2) and is identified as Q in the diffraction patterns. Smaller amounts of mullite ($Al_{2.35}Si_{0.64}O_{4.82}$), hematite ($Fe_2O_3$), magnetite ($Fe_3O_4$), anhydrite ($CaSO_4$), lime ($CaO$), calcite ($CaCO_3$), and periclase ($MgO$) are also present in most samples (Table 1). These results agree with previous measurements which have described fly ash as largely comprised of amorphous material with large amounts of aluminosilicate minerals with some crystalline components.[16] In the XRD diffractograms, CaO peaks were not included because they were found only at the higher angles above 45°. At these higher angles, the components' peaks are often found close together with lower intensities, making them difficult to label in Figure 1. Compared to the large percent composition given by the manufacturer, the XRD results did not show alumina peaks, but we infer that either initially or during the water and acid treatment procedure, the alumina was lost or converted to an amorphous state. No significant change in the overall XRD was observed after water treatment, indicating that any crystalline water-soluble material present is in low amounts. This is expected from previous studies which have revealed the low amounts of water-soluble crystalline components in fly ash.[21, 26, 52]

After acid treatment, gypsum ($Ca(SO_4) \cdot 2H_2O$) is present as a large peak in the diffractogram identified as 'G' (Table 1 and Figure 1) for the Class C and Class C/F fly ash. The water-treated samples have some gypsum present as well but in smaller amounts. The amount of gypsum directly corresponds to the overall amount of Ca in these samples as indicated by Table 1. Even after acid treatment, calcium oxide peaks are still present in the diffraction pattern for these samples indicating that not all of the Ca is available for the reaction and/or is unreactive. The presence of gypsum suggests that the residual sulfuric acid left after centrifugation reacts with the surface of the solid particles. In addition, the Class F Miami sample does not have the same

reactivity as the Class C and C/F samples. The Class F Miami sample has Fe present as hematite and magnetite like the Clifty sample but to a greater extent (Table 1 and Figure 1). These components, along with quartz, compose most of the crystalline material of the treated and untreated Class F Miami sample. Overall, there are no major changes in the Class F Miami sample with water or acid treatment. This result indicates that no crystalline phases are created or altered through these treatments. A small amount of salt formation is possible, but it is likely to be below the detection limit or amorphous.
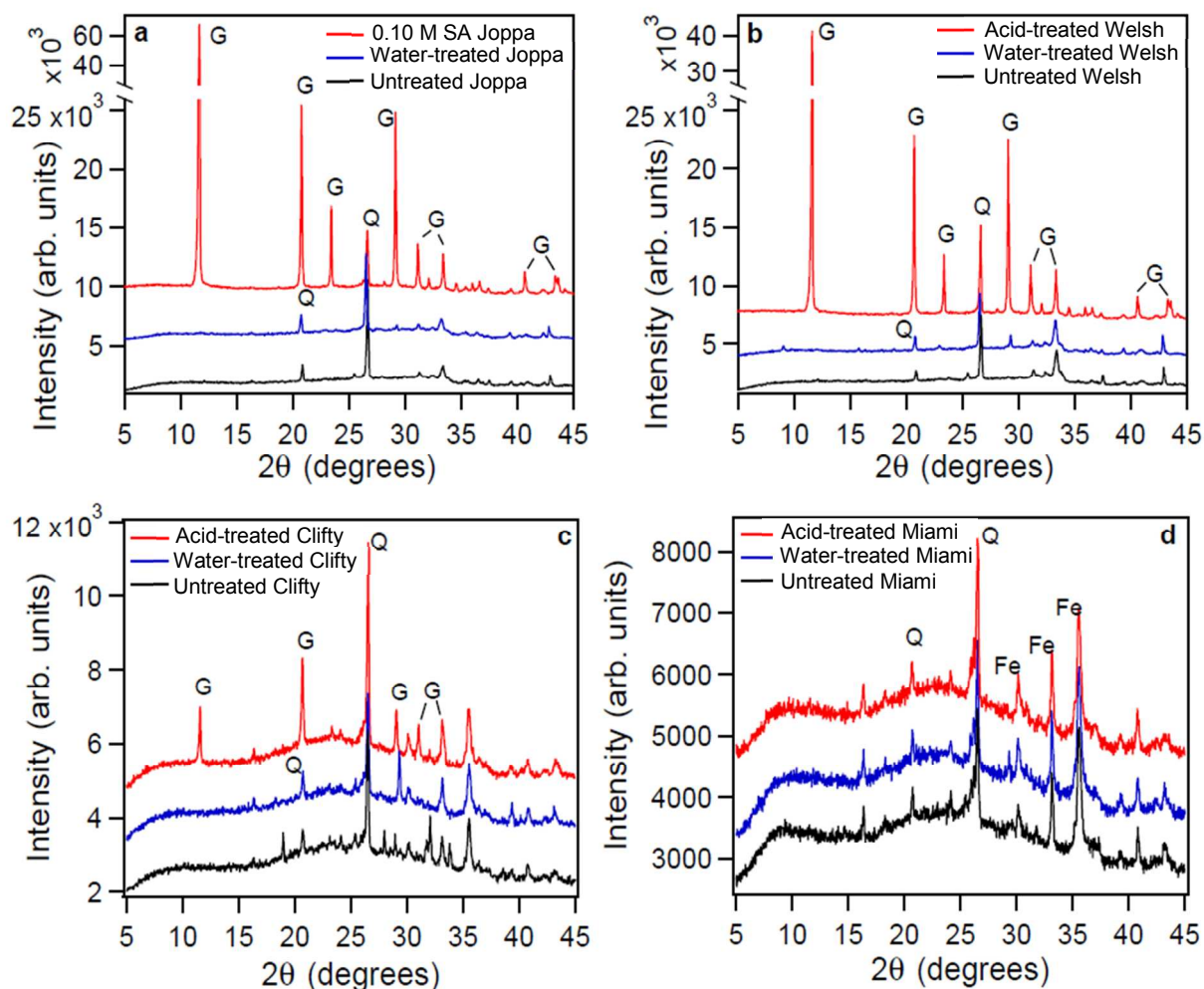
Figure 1. The XRD data for untreated, acid-treated, and water-treated a) Class C Joppa, b) Class C Welsh, c) Class C/F Clifty, and d) Class F Miami fly ash. SA refers to sulfuric acid. Major components, quartz (Q), gypsum (G), and iron oxide (Fe) are marked on each diffraction pattern.

TEM, EDS, and SAED analyses were performed to determine the morphology, elemental composition, and crystallinity of the fly ash types. While XRD shows the average composition over the whole sample, these microscopy analyses characterize individual particles, and therefore demonstrate the heterogeneity of the sample. The SAED images indicate that the samples contain particles, with amorphous and polycrystalline components, as indicated by the diffuse

rings and bright spots, respectively, consistent with silicate glass being a component of fly ash (Figure 2a and 2b). The EDS characterizes the elemental composition of individual particles. For example, our results indicate that Ca, Mg, Al, Si, P, Ti, and Fe are found in Fig. S2a and Si, P, and S are found in Fig. S2b. The presence of Ti was unexpected based on the elemental analysis and XRD results in Table 1; however, small concentrations of Ti are found in the ICP-AES results (Fig. 4) of the Class C/F Clifty sample and TiO_2 has been identified previously in fly ash.[53] Overall, these results are in agreement with the results from Materials Testing Inc. and other studies that performed elemental analysis on fly ash.[21, 28] After acid exposure, large amounts of highly crystalline material appeared throughout the Class C and Class C/F samples, for which a representative particle is shown in Figure 2c. EDS confirms the presence of Ca and S indicating that this particle is likely gypsum, as observed in the XRD (Figure S2c). The EDS spectra (Figure S2d) of the particle in Figure 2d indicates that it is composed of primarily Al and Si with smaller signals from K, Ca, and Fe. The lack of S signal indicates that the gypsum crystals are likely localized or below the detection limit. The Clifty sample behaves like the Class C samples, but with less calcium sulfate observed.
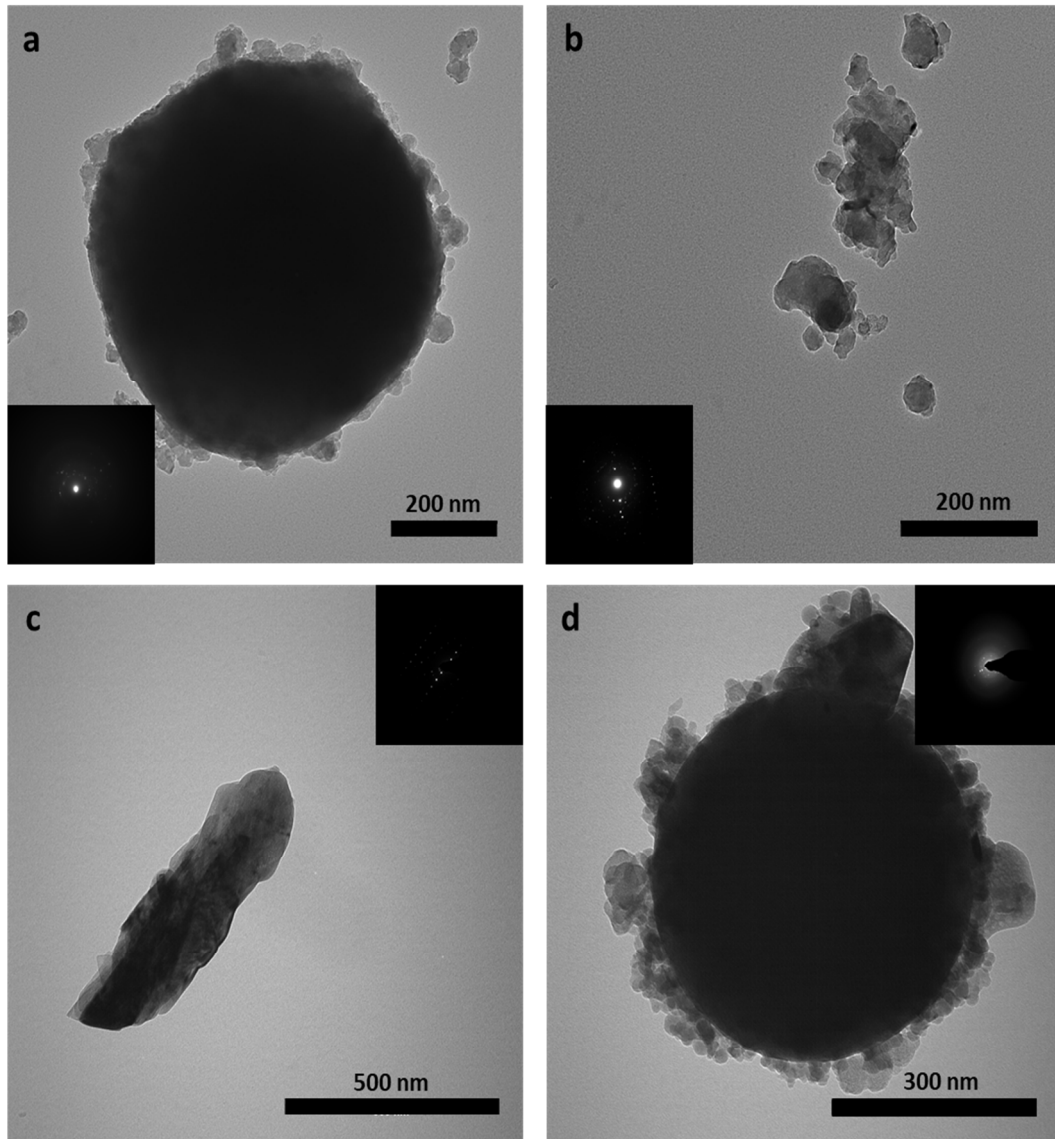
Figure 2. Representative TEM images for the fly ash samples a) spherical, untreated Class C, b) irregular, untreated Class C, c) acid-treated Class C, and d) acid-treated Class C/F. The fly ash particles showed a variety of spherical and irregular particles. Insets are SAED diffractograms showing the degree of crystallinity.

The morphology of the Class F Miami sample as seen in the TEM images in Figure 3 a and b is different from the other fly ash samples. While spheres with small amounts of crystalline

materials around them are observed, fractal structures and more irregular particles with a similar appearance to mineral dust are observed as well (Figure 3 a and b). The fractal structure is composed of Si, Al, S, Ca, and Fe as seen in the EDS spectrum (Figure S3a). The mineral dust-like structure in Figure 3b is primarily composed of Si, Al, Mg, K, and Fe (Figure S3b). After acid treatment, the particle shapes were less distinct, and fewer small particles were observed, perhaps a result of dissolution or agglomeration (Figure 3 c and d). The mineral surface structure after acid treatment appears smoother with less surface defects due to dissolution or particle coatings, and is primarily composed of Si, Al, S, and Fe (Figure S3c), while the spherical particle in Figure 3d is composed of Si, Al, S, K, and Fe (Figure S3d). While XRD results indicate that the Miami sample is less reactive than the other samples, the TEM shows that there are morphological changes as a result of acid treatment.
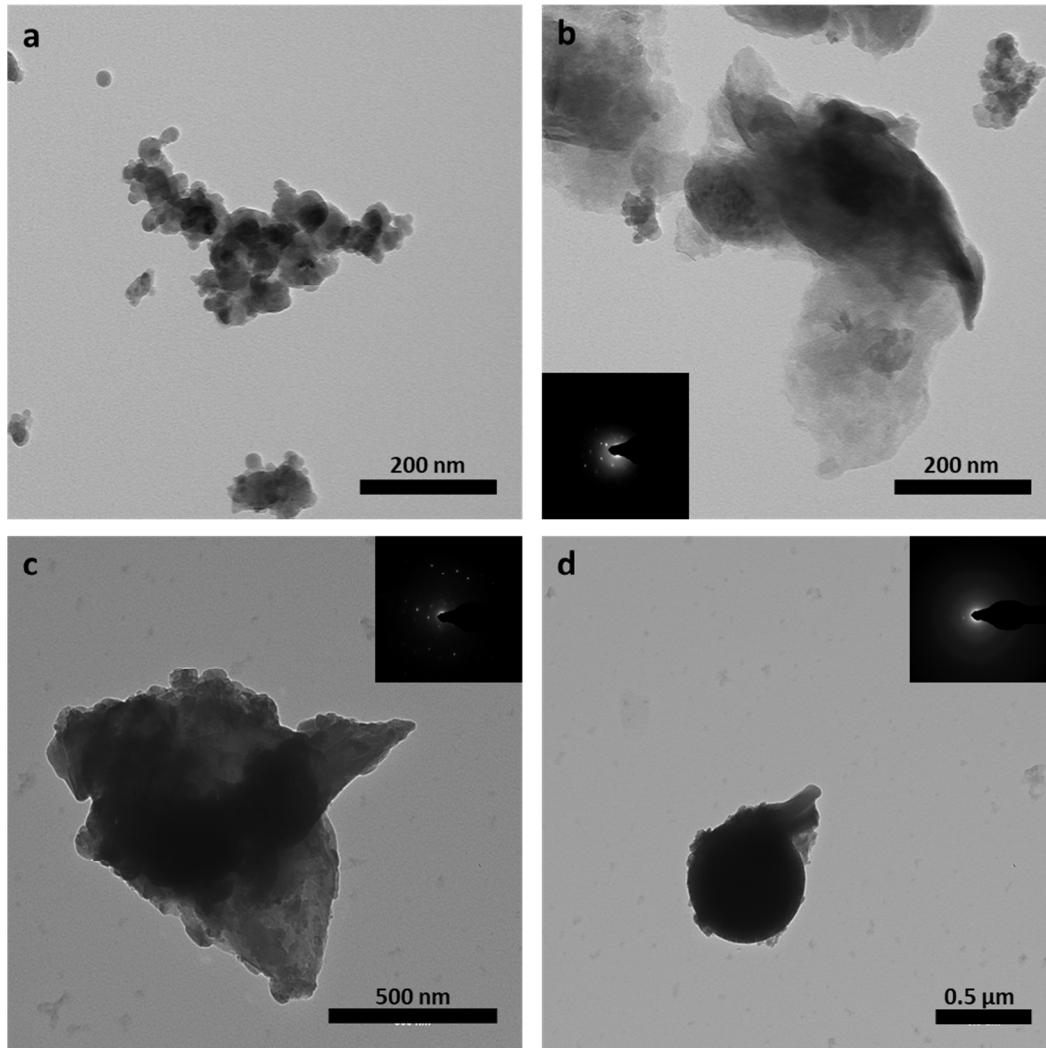
Figure 3. Representative TEM images for Class F Miami fly ash particles (a

and b) and acid-treated Class F Miami fly ash particles (c and d). The insets

are SAED diffractograms showing crystallinity.

ICP-AES analysis was performed on the supernatants to quantitatively examine the leached

ions after water and acid treatment. Note that we list below the major element in these ions rather

than the ion itself; oxides, for example, are not denoted as such. In general, acid treatment

released many more and a greater variety of ions than the water treatment as seen in Figure 4.

This behavior has been observed previously in nitric acid- and sulfuric acid-treated mineral dust

and leaching studies on fly ash.[25, 39, 54] The water treatment released a variety of ions including those containing the elements Ca, S, and Na, with smaller amounts of Al for most of the samples regardless of class. With acid treatment, Class C fly ash released primarily Ca, Mg, Si and Al with some Na. The Class C/F Clifty sample released mainly Na, Ca, Al, and Si, along with some Fe and Mg. The Class F Miami sample released Al, Si, Ca, and Fe with small amounts of Mg and Na, but a much smaller amount was released compared to the other samples, mirroring the low reactivity as reported above for XRD. The release of multiple ions suggests the possibility that a large variety of sulfate salts are formed in addition to gypsum during the drying process, but they are present in too small of an amount or too amorphous to distinguish in the diffractograms. The amounts of ions released do not necessarily reflect the composition of the fly ash outlined in Table 1, but instead are most likely dependent on the availability of the component to react and the chemical environment. Reaction products detected by XRD likely form at the surface of the particles with the residual sulfuric acid that is left on the solid after the supernatant is decanted. The ICP-AES results suggest that Ca is available for reaction to form gypsum because there is a sufficient quantity at the surface to be leached into solution. For Class F, the lack of gypsum could be a result of a lower concentration of CaO in the original fly ash samples. From the ICP-AES data in Figure 4, it can be seen that similar amounts of Ca were leached, which could lead to insufficient Ca in the surface layer for gypsum formation. If calcium sulfate is formed, the amount may be under the XRD detection limit or an amorphous intermediate, which would not have been detected by XRD. In comparison, samples with high Fe content release more Fe during acid treatment.
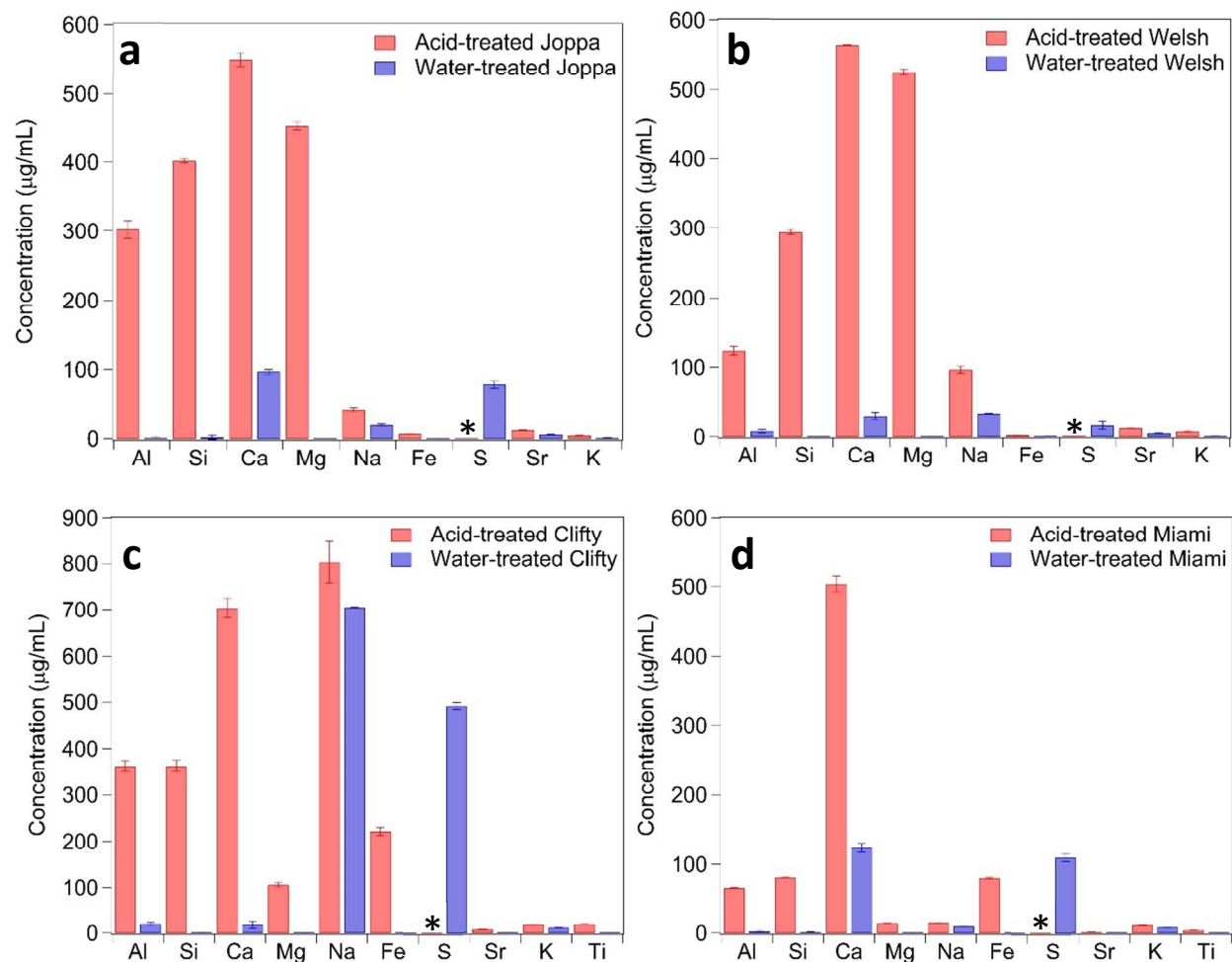
Figure 4. The ICP-AES results for the supernatant collected from the water-treated and acid-treated Class C Joppa and Welsh, Class C/F Clifty, and Class F Miami fly ash samples. Data for S in the acid-treated samples are shown as 0 and marked with an asterisk because the S from the fly ash is masked by the S in the sulfuric acid.

The fate of Fe in the fly ash before and after acidic-processing is of particular interest due to its importance for biogeochemistry.[55] Fly ash has been previously investigated as a source of water soluble Fe. Chen et al. found that, after acidic processing at pH 1 for 1.5 hours, Class F fly ash released about 3 mg Fe/g.[26] Similarly, our ICP-AES results show that the Class F Miami sample released 3.0 mg Fe/g fly ash and Class C/F released 8.3 mg Fe/g fly ash with acid treatment. The Class C fly ash samples Joppa and Welsh released 0.25 and 0.084 g Fe/g fly ash, respectively.

This result is consistent with previous literature on mineral dust, which found that the total iron released does not always correspond to the surface area or the iron content of the sample, indicating that the speciation and chemical environment is necessary to know how much leaching will occur.[56] In addition, Hettiarachchi et al. found that dust samples with high Ti content would have a higher concentration of leached Fe(II) in acidic conditions because of metal-metal synergistic effects.[57] From the ICP-AES results, it is seen that the acid treated Clifty has 20.4 mg/mL Ti leached compared to Miami which had 81.2 mg/mL Ti; therefore, the larger concentration of Ti found in Clifty may have aided the leaching of iron. In the XRD diffractograms, the peaks for hematite (Fe_2O_3) and magnetite (Fe_3O_4) were detected at the higher angles; thus, it could be inferred that both Fe^{2+} and Fe^{3+} were present in the leached solution and on the fly ash samples. The composition and therefore class of the fly ash affects the heterogeneous chemistry and overall environmental impact of the fly ash.

BET analysis was performed to understand how the surface area and pore diameter differs between the water-treated and acid-treated samples (Table 2). Class C fly ash, Joppa and Welsh, and Class F fly ash showed an increase in the surface area of the acid-treated samples compared to the water-treated samples. This can be attributed to acid exposure etching away the edges of particles and infiltrating surface defects, leading to a higher overall surface area. The Class C/F Clifty fly ash showed a slight decrease in surface area with the acid-treated samples. Recent literature has suggested the importance of pore size on ice nucleation behavior,[58-60] and as a result, the pore diameter of each sample was also recorded. For all fly ash samples, the pore diameter was smaller for the acid-treated sample. This result is in contrast to previous studies observing an increase in pore diameter when the aluminosilicate clay minerals, kaolinite and montmorillonite, are treated with sulfuric acid.[61, 62] Fly ash has many different components not

found in kaolinite and montmorillonite and can be even more complex in composition because of the generation processes. This complexity leads to an increase in reactivity, primarily gypsum production and leaching of different metals based on the four fly ash samples studied. The smaller pore diameters could be due to reaction products such as gypsum blocking pore sites, especially in the Class C and Class C/F cases. For Class F, there was no observable formation of gypsum from XRD, and as a result, the pore shrinkage could be the result of crystalline or amorphous reaction products filling the pores (that are not observed with XRD) and/or structural changes to the fly ash. Also of note, there is a large increase in surface area with a decrease in pore size in Class F. This could be a result of the gypsum formation from hemihydrite that has been shown to form air voids from changes in the crystal structure during the transition.[63, 64] If these air voids form close enough to the surface, it would create large defects on the surface, which would increase the surface area. Class C has a larger quantity of CaO initially compared to Class C/F and F, which allows for more hemihydrite to gypsum transformations; thus, there could be more defects at the surface.

Table 2. The BET, pore size, and onset and end of freezing for each fly ash experiment and the reference minerals (quartz and gypsum).

Class	Sample	Treatment	BET (m^2/g)	Pore diameter (nm)	IN Onset (°C)	IN End (°C)
-	Quartz	-	1.344 ± 0.006	-	-13.5	-22.5
-	Gypsum	-	0.416 ± 0.002	-	-19.0	-26.5
Class C	Joppa	Water	8.72 ± 0.05	9.38	-8.0	-30.0
		Acid	21.69 ± 0.06	5.06	-17.5	-28.0
	Welsh	Water	7.8 ± 0.1	9.84	-16.0	-29.5

		Acid	19.58 ± 0.06	6.68	-16.5	-26.0
Class C/F	Clifty	Water	8.88 ± 0.07	7.02	-18.5	-29.0
		Acid	6.24 ± 0.06	5.07	-15.5	-28.0
Class F	Miami	Water	3.92 ± 0.06	5.40	-12.5	-28.5
		Acid	6.2 ± 0.1	3.41	-13.5	-24.0

Table 2 and Figure 5a also show the freezing behavior of each fly ash sample. Immersion freezing analysis was done to determine the effect of the elemental and morphological changes on ice nucleation. Low weight percent suspensions (0.3 wt. %) of the fly ash were prepared to ensure that the fly ash would remain well mixed during the experiments (Table 2). For the fly ash samples, the onset of freezing ranges from -8 to -18.5 ºC, and the last droplet freezes between -24 to -30 ºC. Note that the data found in Table 2 are not normalized by the total surface area of the fly ash within each droplet. These results along with the fraction frozen plot in Figure 5a indicate that all fly ash samples measured showed freezing above the background freezing of the Millipore water, which is indicative of heterogeneous nucleation. The BET results were used to normalize the data for surface area. The background freezing caused by the Millipore water freezing was also accounted for by performing the background subtraction outlined in the Experimental Methods. These results are plotted as the number of ice nucleation active sites as a function of temperature (Figure 5b). The n_s increases monotonically with decreasing temperature except in cases where the Millipore water background freezing outpaces the nucleation due to the fly ash, but heterogeneous nucleation by the fly ash is the predominant mode. Because the freezing events at the beginning and the end can vary slightly between runs, these error bars tend to be large in those areas. Also, in places where the error is greater than the measurement itself, only the positive error is plotted. These results confirm that the Class F Miami acid-treated

sample is a better immersion freezing ice nucleus than both its water-treated counterpart and every other sample. Similarly, the Class C/F Clifty sample also showed better freezing efficiency with the acid-treated sample compared to the water-treated sample. The Class C samples, Joppa and Welsh, however, both show better freezing efficiency with the water-treated samples. Compared to aluminosilicate mineral dust such as kaolinite and Arizona test dust, the fly ash studied in this paper freeze at warmer temperatures overall but also have a lower active site density.[2] Our quartz sample was a more efficient ice nucleus than the fly ash samples. On the other hand, gypsum first nucleated at a later temperature (-19.0 °C) than the fly ash samples and was out-competed by background freezing until -22.0 °C. After this temperature, the number of active sites increased rapidly. Gypsum that was exposed to water for a day and dried showed the same ice nucleation activity as the initial gypsum sample. In Grawe et al. (2018), the work of Garimella was shown.[30, 65] In Garimella's work, the same fly ash samples that were used in the present study were size selected before ice nucleation experiments. Because the fly ash was not size selected for the present study, the ice nucleation results differ from those reported in Garimella, perhaps due to a difference in composition of different size fractions of fly ash.[65]
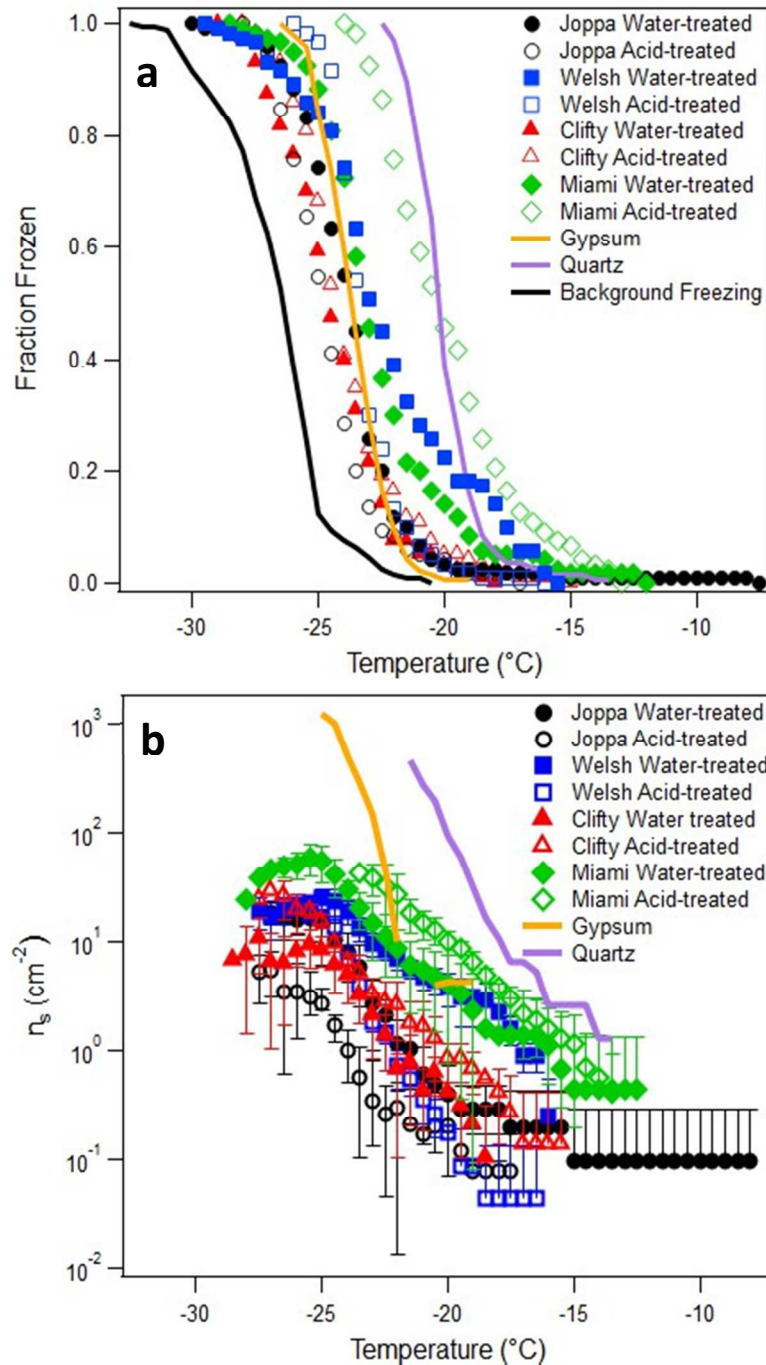
Figure 5. The fraction frozen for the water-treated and acid-treated fly ash samples with the background freezing due to Millipore water (a) and the number of frozen active sites per unit surface area (n_s) plot for each sample with the standard deviation. Gypsum and quartz are added as reference samples.

The differences in freezing efficiency with acid treatment are likely due to the reaction products from acid treatment. When Class C fly ash was treated with sulfuric acid, gypsum was produced and could have blocked sites for ice nucleation during these experiments resulting in a less efficient ice nucleus. Note that the Class C Welsh perhaps shows the most significant decrease in ice nucleation activity. From Figure 5b, it can be seen that although gypsum has a later onset freezing temperature than some of the samples, there is a sharp increase in freezing activity, which indicates that the change in ice nucleation activity of the fly ash samples with the acid treatment is not solely due to composition. Specifically, as a result of gypsum formation, morphological and/or chemical changes at the surface are likely the cause(s) of the differences in ice nucleation. We have previously seen that reaction products created during acid treatment inhibit ice nucleation of aluminosilicate clay minerals.[26] In addition to affecting ice nucleation, gypsum could have impacts on mixed-phase clouds by aiding in the formation of cloud condensation nuclei. Because gypsum is a slightly soluble compound at approximately 0.016 M at 25°C, it has the potential to act as a cloud condensation nucleus if the surface of an aerosol is coated with it.[66]

In contrast to Class C fly ash and previous studies on mineral dust, the sulfuric acid treatment led to better ice nucleation ability for the Class C/F Clifty and Class F Miami samples. Note, the uncertainty in the surface area might account for the trend of these samples. Class C/F and F fly ash both produced little to no crystalline gypsum. The pore size still decreased, which would indicate that reaction products that are amorphous or lower than the detection limit of the XRD could be filling the pores. Additionally, it could be that the pores are not the active sites for this sample. The increase in ice nucleation efficiency could be the result of the acid treatment activating a component such as Fe to become more susceptible to ice nucleation. In addition,

etching of the surface to produce more active sites is likely not the cause of enhancement because the surface area increased for the Class F and decreased for the Class C/F. Our results are therefore inconclusive about why the ice nucleation activity is enhanced after reaction for these samples.

CONCLUSIONS

Sulfuric-acid treatment has major physical and chemical effects on fly ash. These effects are dependent on the class and, therefore, composition of the fly ash. In this paper, acid treatment results in the formation of sulfate salts, namely gypsum, and a variety of metals are leached. In samples where gypsum was produced, the immersion freezing activity decreased. In samples where gypsum was not detected, the immersion freezing activity slightly increased. Our study shows that care should be taken to thoroughly characterize samples because changes in composition across classes of fly ash can lead to very different results in terms of reactivity and ice nucleation activity. Furthermore, the fly ash samples tested, whether acid treated or not, have shown that there is potential for similar particles to serve as ice nuclei and thus have an effect on climate.

AUTHOR INFORMATION

Corresponding Author

*E-mail: maf43@psu.edu

Present Addresses

* To whom all correspondence should be addressed: maf43@psu.edu, 814-867-4267

Author Contributions

The manuscript was written through contributions of all authors. All authors have given approval to the final version of the manuscript.

Conflicts of Interest

The authors declare no competing financial interests.

ACKNOWLEDGMENTS

Electronic Supplemental Information

includes EDS spectra for all fly ash samples, pH measurements, and a representative full XRD diffractogram.

REFERENCES

1. T. Stocker, *Climate Change 2013: The Physical Science Basis. Contribution of Working Group I to the Fifth Assessment Report of the Intergovernmental Panel on Climate Change*, Cambridge University Press, Cambridge, UK, New York, 2014.
2. B. Murray, D. O'sullivan, J. Atkinson and M. Webb, Ice nucleation by particles immersed in supercooled cloud droplets, *Chem. Soc. Rev.*, 2012, **41**, 6519-6554.
3. G. Lesins, P. Chylek and U. Lohmann, A study of internal and external mixing scenarios and its effect on aerosol optical properties and direct radiative forcing, *J. Geophys. Res.-Atmos.*, 2002, **107**, AAC 5-1-AAC 5-12.
4. U. Lohmann and K. Diehl, Sensitivity studies of the importance of dust ice nuclei for the indirect aerosol effect on stratiform mixed-phase clouds, *J. Atmos. Sci.*, 2006, **63**, 968-982.
5. C. Hoose, U. Lohmann, R. Erdin and I. Tegen, The global influence of dust mineralogical composition on heterogeneous ice nucleation in mixed-phase clouds, *Environ. Res. Lett.*, 2008, **3**, 025003.

6. M. Quante, The role of clouds in the climate system, *J. Phys. IV France*, 2004, **121**, 61-86.

7. R. J. Herbert, B. J. Murray, S. J. Dobbie and T. Koop, Sensitivity of liquid clouds to homogenous freezing parameterizations, *Geophys. Res. Lett.*, 2015, **42**, 1599-1605.

8. P. J. DeMott, D. J. Cziczo, A. J. Prenni, D. M. Murphy, S. M. Kreidenweis, D. S. Thomson, R. Borys and D. C. Rogers, Measurements of the concentration and composition of nuclei for cirrus formation, *Proc. Natl. Acad. Sci. U.S.A.*, 2003, **100**, 14655-14660.

9. W. Haag and B. Kärcher, The impact of aerosols and gravity waves on cirrus clouds at midlatitudes, *J. Geophys. Res.-Atmos.*, 2004, **109**, 1-18.

10. K. D. Froyd, D. M. Murphy, P. Lawson, D. Baumgardner and R. L. Herman, Aerosols that form subvisible cirrus at the tropical tropopause, *Atmos. Chem. Phys.*, 2010, **10**, 209-218.

11. D. J. Cziczo, K. D. Froyd, C. Hoose, E. J. Jensen, M. Diao, M. A. Zondlo, J. B. Smith, C. H. Twohy and D. M. Murphy, Clarifying the dominant sources and mechanisms of cirrus cloud formation, *Science*, 2013, **340**, 1320-1324.

12. J. D. Atkinson, B. J. Murray, M. T. Woodhouse, T. F. Whale, K. J. Baustian, K. S. Carslaw, S. Dobbie, D. O'Sullivan and T. L. Malkin, The importance of feldspar for ice nucleation by mineral dust in mixed-phase clouds, *Nature*, 2013, **498**, 355-358.

13. J. Li, M. Pósfai, P. V. Hobbs and P. R. Buseck, Individual aerosol particles from biomass burning in southern Africa: 2, Compositions and aging of inorganic particles, *J. Geophys. Res.-Atmos.*, 2003, **108**, 1-12.

14. M. Pósfai, R. Simonics, J. Li, P. V. Hobbs and P. R. Buseck, Individual aerosol particles from biomass burning in southern Africa: 1. Compositions and size distributions of carbonaceous particles, *J. Geophys. Res.-Atmos.*, 2003, **108**, 1-13.

15. T. C. Bond, S. J. Doherty, D. W. Fahey, P. M. Forster, T. Berntsen, B. J. DeAngelo, M. G. Flanner, S. Ghan, B. Kärcher, D. Koch, S. Kinne, Y. Kondo, P. K. Quinn, M. C. Sarofim, M. G. Schultz, M. Schulz, C. Venkataraman, H. Zhang, S. Zhang, N. Bellouin, S. K. Guttikunda, P. K. Hopke, M. Z. Jacobson, J. W. Kaiser, Z. Klimont, U. Lohmann, J. P. Schwarz, D. Shindell, T. Storelvmo, S. G. Warren and C. S. Zender, Bounding the role of black carbon in the climate system: A scientific assessment, *J. Geophys. Res.-Atmos.*, 2013, **118**, 5380-5552.

16. L. K. A. Sear, ed., *Properties and use of coal fly ash*, Thomas Telford, London, 2001, ch. 1, pp. _-_.

17. J. P. Engelbrecht and E. Derbyshire, Airborne Mineral Dust, *Elements*, 2010, **6**, 241-246.

18. R. T. Chancey, P. Stutzman, M. C. Juenger and D. W. Fowler, Comprehensive phase characterization of crystalline and amorphous phases of a Class F fly ash, *Cement Concrete Res.*, 2010, **40**, 146-156.

19. ASTM International, *Standard test methods for sampling and treating fly ash of natural pozzolans for use in Portland-cement concrete*, 2013.

20. J. G. Navea, E. Richmond, T. Stortini and J. Greenspan, Water adsorption isotherms on fly ash from several sources, *Langmuir*, 2017, **33**, 10161-10171.

21. F. Parungo, E. Ackerman, H. Proulx and R. Pueschel, Nucleation properties of fly ash in a coal-fired power-plant plume, *Atmos. Environ.*, 1978, **12**, 929-935.

22. J. Inoue, A. Momose, T. Okudaira, A. Murakami-Kitase, H. Yamazaki and S. Yoshikawa, Chemical characteristics of Northeast Asian fly ash particles: Implications for their long-range transportation, *Atmos. Environ.*, 2014, **95**, 375-382.

23. W. Li, L. Shao, Z. Shi, J. Chen, L. Yang, Q. Yuan, C. Yan, X. Zhang, Y. Wang and J. Sun, Mixing state and hygroscopicity of dust and haze particles before leaving Asian continent, *J. Geophys. Res.-Atmos.*, 2014, **119**, 1044-1059.

24. S. Nagib and K. Inoue, Recovery of lead and zinc from fly ash generated from municipal incineration plants by means of acid and/or alkaline leaching, *Hydrometallurgy*, 2000, **56**, 269-292.

25. M. Izquierdo and X. Querol, Leaching behaviour of elements from coal combustion fly ash: An overview, *Int. J. Coal Geol.*, 2012, **94**, 54-66.

26. H. Chen, A. Laskin, J. Baltrusaitis, C. A. Gorski, M. M. Scherer and V. H. Grassian, Coal fly ash as a source of iron in atmospheric dust, *Environ. Sci. Technol.*, 2012, **46**, 2112-2120.

27. N. Hiranuma, N. Hoffmann, A. Kiselev, A. Dreyer, K. Zhang, G. Kulkarni, T. Koop and O. Möhler, Influence of surface morphology on the immersion mode ice nucleation efficiency of hematite particles, *Atmos. Chem. Phys.*, 2014, **14**, 2315-2324.

28. N. S. Umo, B. J. Murray, M. T. Baeza-Romero, J. M. Jones, A. R. Lea-Langton, T. L. Malkin, D. O'Sullivan, L. Neve, J. M. C. Plane and A. Williams, Ice nucleation by combustion ash particles at conditions relevant to mixed-phase clouds, *Atmos. Chem. Phys.*, 2015, **15**, 5195-5210.

29. S. Grawe, S. Augustin-Bauditz, S. Hartmann, L. Hellner, J. B. C. Pettersson, A. Prager, F. Stratmann and H. Wex, The immersion freezing behavior of ash particles from wood and brown coal burning, *Atmos. Chem. Phys.*, 2016, **16**, 13911-13928.

30. S. Grawe, S. Augustin-Bauditz, H.-C. Clemen, M. Ebert, S. Eriksen Hammer, J. Lubitz, N. Reicher, Y. Rudich, J. Schneider and R. Staacke, Coal fly ash: linking immersion freezing behavior and physicochemical particle properties, *Atmos. Chem. Phys.*, 2018, **18**, 13903-13923.

31. M. A. Zawadowicz, K. D. Froyd, D. M. Murphy and D. J. Cziczo, Improved identification of primary biological aerosol particles using single-particle mass spectrometry, *Atmos. Chem. Phys.*, 2017, **17**, 7193-7212.

32. F. Blanco, M. Garcia and J. Ayala, Variation in fly ash properties with milling and acid leaching, *Fuel*, 2005, **84**, 89-96.

33. M. L. Eastwood, S. Cremel, M. Wheeler, B. J. Murray, E. Girard and A. K. Bertram, Effects of sulfuric acid and ammonium sulfate coatings on the ice nucleation properties of kaolinite particles, *Geophys. Res. Lett.*, 2009, **36**, 1-5.

34. R. Sullivan, M. Petters, P. DeMott, S. Kreidenweis, H. Wex, D. Niedermeier, S. Hartmann, T. Clauss, F. Stratmann and P. Reitz, Irreversible loss of ice nucleation active sites in mineral dust particles caused by sulphuric acid condensation, *Atmos. Chem. Phys.*, 2010, **10**, 11471-11487.

35. D. I. Chernoff and A. K. Bertram, Effects of sulfate coatings on the ice nucleation properties of a biological ice nucleus and several types of minerals, *J. Geophys. Res.-Atmos.*, 2010, **115**, 1-12.

36. D. Niedermeier, S. Hartmann, R. Shaw, D. Covert, T. Mentel, J. Schneider, L. Poulain, P. Reitz, C. Spindler and T. Clauss, Heterogeneous freezing of droplets with immersed mineral dust particles–measurements and parameterization, *Atmos. Chem. Phys.*, 2010, **10**, 3601-3614.

37. Z. Yang, A. K. Bertram and K. C. Chou, Why do sulfuric acid coatings influence the ice nucleation properties of mineral dust particles in the atmosphere?, *J. Phys. Chem. Lett.*, 2011, **2**, 1232-1236.

38. Y. Tobo, P. J. DeMott, M. Raddatz, D. Niedermeier, S. Hartmann, S. M. Kreidenweis, F. Stratmann and H. Wex, Impacts of chemical reactivity on ice nucleation of kaolinite particles: A case study of levoglucosan and sulfuric acid, *Geophys. Res. Lett.*, 2012, **39**, 1-5.

39. S. K. Sihvonen, G. P. Schill, N. A. Lyktey, D. P. Veghte, M. A. Tolbert and M. A. Freedman, Chemical and physical transformations of aluminosilicate clay minerals due to acid treatment and consequences for heterogeneous ice nucleation, *J. Phys. Chem. A*, 2014, **118**, 8787-8796.

40. H. Guo, L. Xu, A. Bougiatioti, K. M. Cerully, S. L. Capps, J. R. Hite Jr, A. G. Carlton, S. H. Lee, M. H. Bergin, N. L. Ng, A. Nenes and R. J. Weber, Fine-particle water and pH in the southeastern United States, *Atmos. Chem. Phys.*, 2015, **15**, 5211-5228.

41. H. Guo, A. P. Sullivan, P. Campuzano-Jost, J. C. Schroder, F. D. Lopez-Hilfiker, J. E. Dibb, J. L. Jimenez, J. A. Thornton, S. S. Brown and A. Nenes, Fine particle pH and the partitioning of nitric acid during winter in the northeastern United States, *J. Geophys. Res.-Atmos.*, 2016, **121**.

42. A. Bougiatioti, P. Nikolaou, I. Stavroulas, G. Kouvarakis, R. Weber, A. Nenes, M. Kanakidou and N. Mihalopoulos, Particle water and pH in the eastern Mediterranean: source variability and implications for nutrient availability, *Atmos. Chem. Phys.*, 2016, **16**, 4579-4591.

43. M. Liu, Y. Song, T. Zhou, Z. Xu, C. Yan, M. Zheng, Z. Wu, M. Hu, Y. Wu and T. Zhu, Fine particle pH during severe haze episodes in northern China, *Geophys. Res. Lett.*, 2017, **44**, 5213-5221.

44. M. F. De Lange, T. J. Vlugt, J. Gascon and F. Kapteijn, Adsorptive characterization of porous solids: Error analysis guides the way, *Micropor. and Mesopor. Mat.*, 2014, **200**, 199-215.

45. D. P. Veghte, J. E. Moore, L. Jensen and M. A. Freedman, Influence of shape on the optical properties of hematite aerosol, *J. Geophys. Res.-Atmos.*, 2015, **120**, 7025-7039.

46. D. P. Veghte, M. B. Altaf, J. D. Haines and M. A. Freedman, Optical properties of non-absorbing mineral dust components and mixtures, *Aerosol Sci. Tech.*, 2016, **50**, 1239-1252.

47. S. K. Sihvonen, K. A. Murphy, N. M. Washton, M. B. Altaf, K. T. Mueller and M. A. Freedman, Effect of acid on surface hydroxyl groups on kaolinite and montmorillonite, *Z. Phys. Chem.*, 2018, **232**, 409-430.

48. V. J. Alstadt, J. N. Dawson, D. J. Losey, S. K. Sihvonen and M. A. Freedman, Heterogeneous freezing of carbon nanotubes: A model system for pore condensation and freezing in the atmosphere, *J. Phys. Chem. A*, 2017, **121**, 8166-8175.

49. S. L. Broadley, B. J. Murray, R. J. Herbert, J. D. Atkinson, S. Dobbie, T. L. Malkin, E. Condliffe and L. Neve, Immersion mode heterogeneous ice nucleation by an illite rich powder representative of atmospheric mineral dust, *Atmos. Chem. Phys.*, 2012, **12**, 287-307.

50. G. Vali, Quantitative evaluation of experimental results an the heterogeneous freezing nucleation of supercooled liquids, *J. Atmos. Sci.*, 1971, **28**, 402-409.

51. D. O′Sullivan, B. J. Murray, J. F. Ross, T. F. Whale, H. C. Price, J. D. Atkinson, N. S. Umo and M. E. Webb, The relevance of nanoscale biological fragments for ice nucleation in clouds, *Sci. Rep.-UK*, 2015, **5**, 8082.

52. X. Querol, J. C. UmaNa, A. Alastuey, C. Bertrana, A. Lopez-Soler and F. Plana, Extraction of water-soluble impurities from fly ash, *Energ. Source.*, 2000, **22**, 733-749.

53. O. O. Fatoba, L. F. Petrik, W. M. Gitari and E. I. Iwuoha, Fly ash-brine interactions: Removal of major and trace elements from brine, *J. Environ. Sci. Heal. A.*, 2011, **46**, 1648-1666.

54. B.-M. Steenari, S. Schelander and O. Lindqvist, Chemical and leaching characteristics of ash from combustion of coal, peat and wood in a 12 MW CFB–a comparative study, *Fuel*, 1999, **78**, 249-258.

55. T. Jickells, Z. An, K. K. Andersen, A. Baker, G. Bergametti, N. Brooks, J. Cao, P. Boyd, R. Duce and K. Hunter, Global iron connections between desert dust, ocean biogeochemistry, and climate, *Science*, 2005, **308**, 67-71.

56. D. M. Cwiertny, J. Baltrusaitis, G. J. Hunter, A. Laskin, M. M. Scherer and V. H. Grassian, Characterization and acid-mobilization study of iron-containing mineral dust source materials, *J. Geophys. Res.-Atmos.*, 2008, **113**, 1-18.

57. E. Hettiarachchi, R. L. Reynolds, H. L. Goldstein, B. Moskowitz and G. Rubasinghege, Iron dissolution and speciation in atmospheric mineral dust: Metal-metal synergistic and antagonistic effects, *Atmos. Environ.*, 2018, **187**, 417-423.

58. C. Marcolli, Deposition nucleation viewed as homogeneous or immersion freezing in pores and cavities, *Atmos. Chem. Phys.*, 2014, **14**, 2071-2104.

59. C. Gurganus, J. Charnawskas, A. Kostinski and R. Shaw, Nucleation at the contact line observed on nanotextured surfaces, *Phys. Rev. Lett.*, 2014, **113**, 235701.

60. T. F. Whale, M. A. Holden, A. N. Kulak, Y.-Y. Kim, F. C. Meldrum, H. K. Christenson and B. J. Murray, The role of phase separation and related topography in the exceptional ice-nucleating ability of alkali feldspars, *Phys. Chem. Chem. Phys.*, 2017, **19**, 31186-31193.

61. P. Kumar, R. V. Jasra and T. S. Bhat, Evolution of porosity and surface acidity in montmorillonite clay on acid activation, *Ind. Eng. Chem. Res.*, 1995, **34**, 1440-1448.

62. A. K. Panda, B. G. Mishra, D. K. Mishra and R. K. Singh, Effect of sulphuric acid treatment on the physico-chemical characteristics of kaolin clay, *Colloid Surface A*, 2010, **363**, 98-104.

63. F. Lea and R. Nurse, Problems of crystal growth in building materials, *Discuss. Faraday Soc.*, 1949, **5**, 345-351.

64. M. Santhanam, M. D. Cohen and J. Olek, Effects of gypsum formation on the performance of cement mortars during external sulfate attack, *Cement Concrete Res.*, 2003, **33**, 325-332.

65. S. Garimella, Ph.D. Thesis, Massachusetts Institute of Technology, 2016.

66. A. Lebedev and V. Kosorukov, Gypsum solubility in water at 25° C, *Geochem. Int+*, 2017, **55**, 205-210.

1
2
3
4
5
6
7
8
9
10
11
12
13
14
15
16
17
18
19
20
21
22
23
24
25
26
27
28
29
30
31
32
33
34
35
36
37
38
39
40
41
42
43
44
45
46
47
48
49
50
51
52
53
54
55
56
57
58
59
60

TOC Image
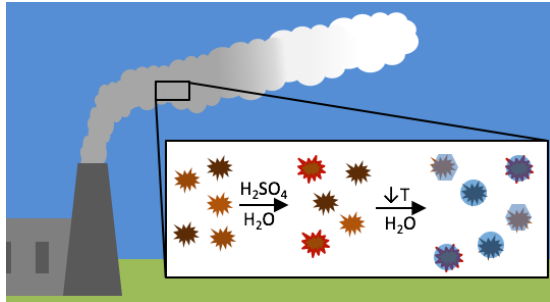
The ice nucleation activity of fly ash, a byproduct of coal combustion, depends on its composition.